IEEE Access
Multidisciplinary | Rapid Review | Open Access Journal

Received May 23, 2018, accepted July 6, 2018, date of publication July 19, 2018, date of current version August 15, 2018.

Digital Object Identifier 10.1109/ACCESS.2018.2857472

Liquid-Metal-Fluidically Switchable Metasurface for Broadband and Polarization-Insensitive Absorption

DAECHEON LIM AND SUNGJOON LIM
School of Electrical and Electronics Engineering, Chung-Ang University, Heukseok-Dong, Seoul 156-756, South Korea

Corresponding author: Sungjoon Lim (sungjoon@cau.ac.kr)

This work was supported by the National Research Foundation of Korea through the Korean Government (MSIP) under Grant 2017R1A2B3003856.

ABSTRACT This paper proposes a switchable metasurface for broadband and polarization-insensitive absorption, whose absorption spectrum can be fluidically switched using liquid metal. The proposed metasurface consists of a top metallic pattern, a flexible printed circuit board substrate, a polydimethylsiloxane substrate, and a bottom metallic ground plane. The proposed unitcell is inspired by a four-circular-sector structure. To maintain the symmetrical geometry and increase the switching range, a symmetrical microfluidic channel is designed with a circular ring capillary and four isolated patches. To measure the absorptivity of the proposed metasurface, 10 × 10 unitcells are fabricated with 20 inlets and 20 outlets. When the microfluidic channels of the metasurface are empty, the fabricated metasurface achieves an absorptivity of higher than 90%, from 6.23 to 12.14 GHz. When eutectic gallium–indium alloy is injected into the microfluidic channels, the fabricated metasurface achieves higher than 90% absorptivity, from 5.44 to 6.12 GHz. Thus, for both cases, the absorptivity is constant at different incident polarization angles.

INDEX TERMS
Metamaterial, electromagnetic absorber, switchable, microfluidic channel, broadband, liquid metal.

I. INTRODUCTION

A metamaterial can artificially control electromagnetic properties such as permittivity and permeability through a periodic arrangement of the resonant structure [1]. The properties of a metamaterial have been applied to various fields, such as super lenses, antennas, and recently, electromagnetic wave-absorbable metasurfaces [2]–[9]. The principle of an electromagnetic wave-absorbable metasurface is to periodically arrange the resonators such that the intrinsic impedance of the metasurface equals that of air. On reaching this equivalence, normal incident electromagnetic waves are permeated on the metasurface without being reflected at the interface and are attenuated owing to the loss of the dielectric material.10 The characteristics of such a metasurface enable the achievement of high absorptivity despite the use of a smaller thickness than that used in wedge-tapered absorbers or Jaumann absorbers thus far [11], [12]. However, the use of resonators causes the metasurface to operate only within a narrow band. To address this issue, a multi-band, wide-band, and switchable metasurface has been studied [13]–[15]. Among the methods used to form a broadband metasurface, a typical method uses resistive or lossy components [16]. By adding resistive components to the unitcell structure of a metasurface, the range of its absorption spectrum can be increased by reducing the quality factor (Q) of the resonator. On the other hand, methods for switching the frequency band of a metasurface have also been studied, using diodes, liquid crystals, micro-electromechanical systems (MEMs), VO2, BST, graphene, and microfluidic channels [17]–[23]. Of these, the use of microfluidic channels is relatively simple and cost-effective compared to other switching methods. However, when creating symmetrical structures, the use of microfluidic channels has certain limitations owing to the need for inlets and outlets allowing the liquids to flow inside, [24] which creates a polarization-sensitive absorption problem in a metasurface with microfluidic channels. To solve this problem, we propose a structure that minimizes the influence of the inlet and outlet parts by using a microfluidic channel as a switch for connecting the metallic patterns. In this case, it is possible to design a microfluidic metasurface insensitive to

polarization if the parts affecting the actual operation, except for the inlet and outlet, are designed with a symmetrical structure.

This paper proposes a switchable wideband metasurface using a microfluidic channel and liquid metal. The proposed metasurface originates from the resistive four-circular sector as a resonant unitcell for broadband absorption and incident angle insensitivity [25], [26]. To switch the absorption spectrum, liquid metal is injected into the microfluidic channel on the resonant unit cell. To maintain the symmetrical geometry and increase the wide switching range, a symmetrical microfluidic channel is designed with a circular ring capillary and four isolated patches. Therefore, the proposed metasurface achieves a wide absorption spectrum, wide frequency-switching capability, polarization insensitivity, and angle insensitivity. The performances of the proposed absorber are compared with those of other previous absorbers.

II. DESIGN AND SIMULATION

Figure 1 shows the unitcell design of the proposed metasurface. The unitcell was designed based on a four-circular-sector structure with a chip resistor, as shown in Figure 1a. The four-circular-sector structure is insensitive to polarization and the incident angle owing to its symmetrical and circular design, and the added chip resistor can allow the metasurface to achieve a wide absorption spectrum range. Figure 1b shows the proposed metasurface's top metallic pattern with a chip resistor. The metallic pattern consists of a four-circular-sector structure in the centre and isolated patches surrounding the sector. A chip resistor is added to the gap between the four-circular sector and isolated patches to achieve a spectrum with a wide absorption range. The resistance of the chip resistors in the four-circular sector and isolated patches is 150 and 20 ohm, respectively. Figure 1c shows the microfluidic channel of the proposed metasurface. The microfluidic channel consists of four circular rings and passages. The circular rings are designed to be symmetrical, and thus, are insensitive to polarization. The passages for connecting the four rings are designed so that there is minimal effect on the performance. Figure 1d shows the top view of the proposed unitcell of the proposed metasurface, which has a nearly symmetrical structure. When the microfluidic channel is empty, the four-circular sector and isolated patches are not connected. On the other hand, when liquid metal is injected into the microfluidic channel, the two are connected with a microfluidic channel. The graph in Figure 1e shows the effect on absorption spectrum of the microfluidic channel. The absorption spectrum of the four-circular-sector metasurface operates in the X-band. The absorption spectrum of the proposed metasurface with an empty microfluidic channel, in which the four-circular sector with isolated patches operates in the X-band owing to the presence of disconnected isolated patches, has little effect on its frequency range. When liquid metal is injected into the microfluidic channel and the four-circular sector and isolated patches are connected, the frequency range of the absorption spectrum is switched from the X-band to the C-band. The parameters in Figure 1 are determined as $G_c = 0.5$, $L_c = 5.4$, $L_s = 0.7$, $P_c = 4.25$, $D_r = 6.15$, $L_i = 6$, $L_o = 8.5$, $L_r = 1$, $W_o = 2.5$, $W_r = 1.5$, $L_w = 3.9$, $L_l = 9.6$, $P_c = 5.3$, $W_c = 1.7$, $W_w = 0.5$ mm, and $A_o = 40°$.

Figure 2a shows the 3D view of a unitcell of the proposed metasurface. The metallic pattern and chip resistors are located on a 0.1-mm-thick flexible printed circuit board (FPCB) substrate [27]. The relative permittivity and loss tangent of the FPCB substrate are 3.5 and 0.04, respectively. The microfluidic channel is implemented in polydimethylsiloxane (PDMS) with a thickness, Tp, of 3.1 mm and the channel depth is about 0.4 mm [28], [29]. The permittivity and loss tangent of the PDMS substrate used are 3 and 0.065, respectively. A 0.05-mm-thick adhesive film is used to attach the FPCB substrate to the PDMS substrate. At the bottom, the metallic plate serves as the ground. The design of the full-sized metasurface is shown in Figure 2b, where a 10 × 10 unitcell is arranged. On the outside of the unitcell array, 20 inlets and 20 outlets for liquid metal injection are

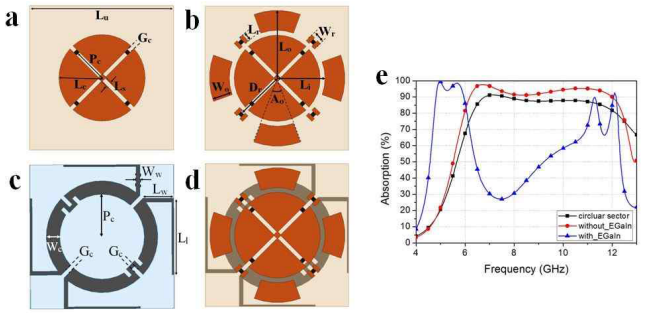

FIGURE 1. Unitcell design of (a) primitive resistive four-circular sector, (b) metallic pattern of proposed metasurface without microfluidic channels, (c) only microfluidic channels, (d) top pattern with the microfluidic channels of the proposed metasurface, and (e) simulation results of the proposed metasurface.

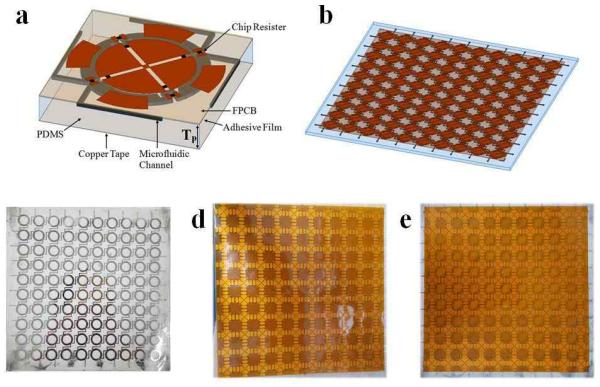

FIGURE 2. 3D view of (a) unitcell of proposed metasurface, (b) 10 × 10 sample of proposed metasurface, (c) fabricated microfluidic channel layer, and the fabricated sample (d) without and (e) with EGaIn.

implemented. Figure 2c–e shows the developed metasurface samples.

Figure 2c shows a fabricated microfluidic channel injected with liquid metal. The microfluidic channel is realized by laser printing on a PDMS of 3.1 mm thickness and 200 mm × 200 mm area. Eutectic gallium indium alloy (EGaIn) is used as the liquid metal [30]. Figure 2d shows the fabricated metasurface sample. The copper patterns and chip resistors are fabricated on a 180 mm × 180 mm FPCB substrate, which is made of polyamide [31]. Figure 2e shows a sample of the proposed metasurface in which EGaIn is injected into the microfluidic channel. The bottom metallic ground plane is realized using a copper tape.

Figure 3 shows the simulation results of the proposed metasurface when one parameter is varied and the others are fixed as $G_c = 0.5, L_c = 5.4, L_s = 0.7, P_c = 4.25, D_r = 6.15, L_i = 6, L_o = 8.5, L_r = 1, W_o = 2.5, W_r = 1.5, L_w = 3.9, L_l = 9.6, P_c = 5.3, W_c = 1.7, W_w = 0.5$ mm, and $A_o = 40°$.

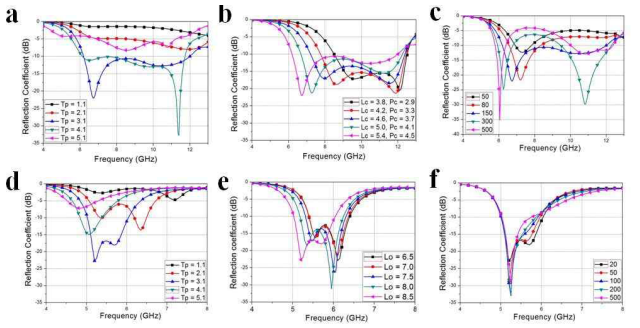

FIGURE 3. Simulation results of proposed metasurface without liquid metal for different (a) T_p (b) L_c and P_c, (c) resistance of chip resistor in four-circular sector and with liquid metal for different (d) T_p and (e) L_o and L_s, and (f) resistance of chip resistor in isolated patches.

The graphs in Figure 3c show the reflection coefficient when the microfluidic channel is empty. Figure 3a shows the change in thickness of the substrate T_p when the other parameters are fixed. When the thickness of PDMS is 3.1 or 4.1 mm, the reflection coefficient is less than -10 dB; however, the reflection coefficient is over -10 dB at the other thicknesses. Figure 3b shows the change in radius of the four-circular sector, L_c, and the location of the chip resistor, Pc, on the circular sector when the other parameters are fixed. As L_c increases, the minimum frequency of the absorption spectrum decreases. Figure 3c shows the change in resistance of the chip resistor on the four-circular sector when the other parameters are fixed. When the resistance is too small, the absorption is lowered to around 10 GHz, and when the resistance is too large, the absorption rate is lowered to around 8 GHz. The proposed metasurface has a chip resistance of 150 ohms, thereby satisfying the demand of a wide absorption spectrum. The graphs in Figure 3d–f show the reflection coefficient when liquid metal is injected in the microchannel. Figure 3d shows the change in T_p when the other parameters are fixed. When T_p is 3.1 mm, the widest absorption spectrum occurs. The graphs in Figure 3e show the change in L_o. As Lo increases, the minimum frequency of the absorption spectrum decreases. Figure 3f shows the change in resistance of the chip resistor in isolated patches when the other parameters are fixed. As the resistance of the chip resistor in the isolated patches decreases, the range of the absorption spectrum increases.

Figure 4 shows the change in performance when the polarization and incident angles of the proposed metasurface are changed. Figure 4a and 4b shows the absorption spectrum for an empty microfluidic channel of the proposed metasurface for different polarizations and incident angles, respectively. When liquid metal is not injected, because the unitcell of the proposed metasurface is symmetrical with respect to the four directions, even when the polarization changes, the absorption spectrum does not change, as indicated in Figure 4a. In this case, the proposed metasurface is insensitive to changes in the incident angle because the unitcell of the four-circular sector, based on the proposed metasurface, is insensitive to the incident angle. Figure 4b shows that the proposed metasurface has an absorptivity of over 80% from 6 to 12 GHz when the incident angle is less than 40°. Figure 4c and 4d shows the absorption spectrum when liquid metal is injected into the microfluidic channel of the proposed metasurface for different polarizations and incident angles, respectively. Figure 4c shows that the proposed metasurface operates at 5–6 GHz when the polarization of the incident electromagnetic waves is zero or 90°. However, when the polarization is not zero or 90°, the absorption spectrum changes, and it is confirmed that the proposed metasurface operates at 5 to 5.4 GHz when the polarization of the incident electromagnetic waves is 30 or 60° and at 5.4 to 6 GHz when the polarization is 120 or 150°. The absorption spectrum of the proposed metasurface is affected by the incident angle. As the incident angle increases, the range of the

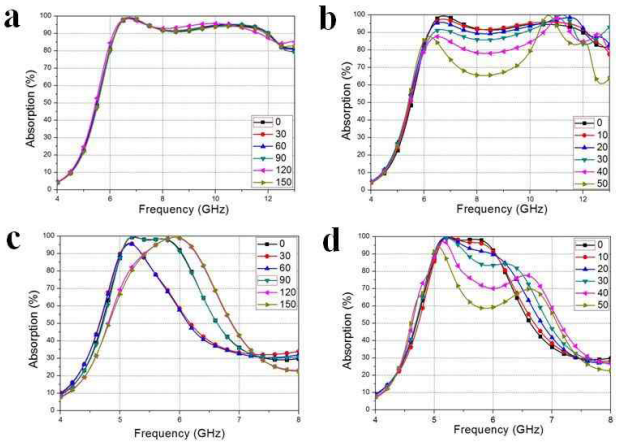

FIGURE 4. Simulation results of proposed metasurface without liquid metal for different (a) polarizations at normal incidence and (b) incident angles with liquid metal for different (c) polarizations at normal incidence and (d) incident angles.

absorption spectrum increases and the absorption decreases. Figure 4d shows that the proposed metasurface has an absorption value above 80% from 5 to 6 GHz when the incident angle is less than 30°.

Figure 5 shows the magnitude of electric-field distribution at the two peak frequencies of the proposed metasurface. Figure 5a and 5b shows the magnitude of electric-field distribution when liquid metal is not injected at 6.7 or 10.4 GHz, respectively. At 6.7 GHz, the electric field is mainly distributed at the edge and the resistor of the four-circular sector. At 10.4 GHz, the electric field is mainly distributed around the resistor of the four-circular sector. According to the above distribution, when liquid metal is not injected into the microfluidic channel, the size of the four-circular sector affects the lower resonance of the proposed metasurface and the resistance affects both resonances of the proposed metasurface. This can be seen in Figure 3b and 3c. Figure 5a and 5b shows the electric-field distribution when liquid metal is injected at 5.2 or 5.7 GHz, respectively. At 5.2 GHz, the electric field is mainly distributed at the edge of the four-circular sector and in isolated patches. At 5.2 GHz, the electric field is mainly distributed around the resistor in isolated patches. From the above distribution, when liquid metal is injected into the microfluidic channel, the size of the isolated patches affects the low resonance of the proposed metasurface, while the resistance affects the high resonance. This can be seen in Figure 3e and 3f.

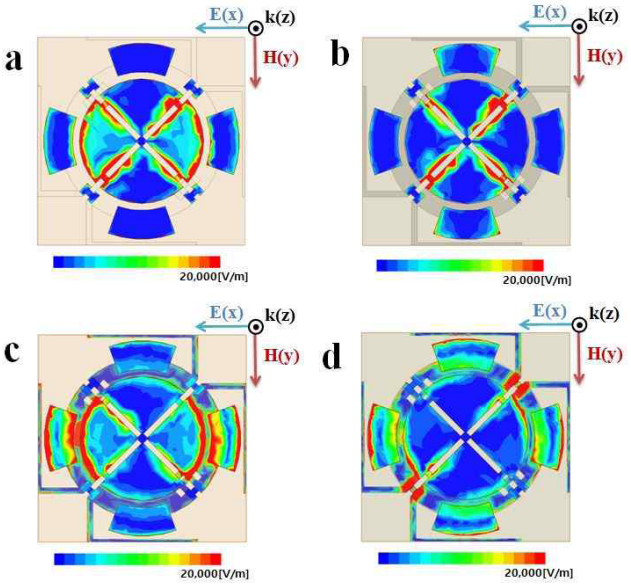

FIGURE 5. Magnitude of electric-field distribution of proposed metasurface without liquid metal at (a) 6.7 GHz and (b) 10.4 GHz, with liquid metal at (c) 5.2 GHz and (d) 5.7 GHz.

III. MEASUREMENT RESULTS

Figure 6 shows the measurement setup used for the proposed metasurface. A wedge-tapered absorber was installed on the back of the sample to prevent signal reflection from occurring

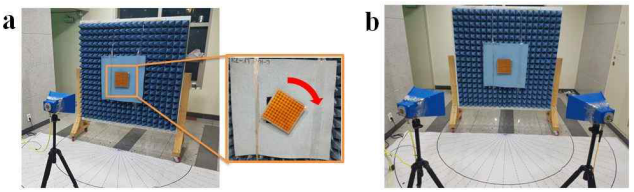

FIGURE 6. Measurement setup for different (a) polarizations and (b) incident angles.

outside the sample, and a comparative analysis was conducted using a copper plate of the same size as that of the sample to determine the absorption of the proposed metasurface. The sample was measured using a horn antenna at a distance of 1.5 mm from the sample in order to meet the far-field condition. Figure 6a shows the measurement setup for different polarizations at normal incidence. By rotating the sample using a holder, we could measure the sample's performance at different polarization angles. The sample was measured by rotating the polarization angle from zero to 180° at 30° intervals. Figure 6b shows the measurement setup for an incident angle. Using two horn antennas and a change in their location, we could measure the sample's performance at different incident angles. The samples were measured through a change in the incident angle from 0 to 50° at 50° intervals.

Figure 7 shows the measurement results of a fabricated sample of the proposed metasurface. First of all, Figure 7a compares the simulation and measurement results at normal incidence. When liquid metal was not injected, the absorption spectrum of the proposed absorber did not differ between the simulation and measurement results. When EGaIn was injected into the microfluidic channel, the absorption spectrum of the proposed metasurface differed between the simulation and measurement results, which is attributed to the two resonances of the proposed metasurface being closer in the case of the simulation. Figure 7b and 7c shows the measurement results of a sample without EGaIn for different polarizations and incident angles, respectively. When the polarization was changed from zero to 180° , the absorption

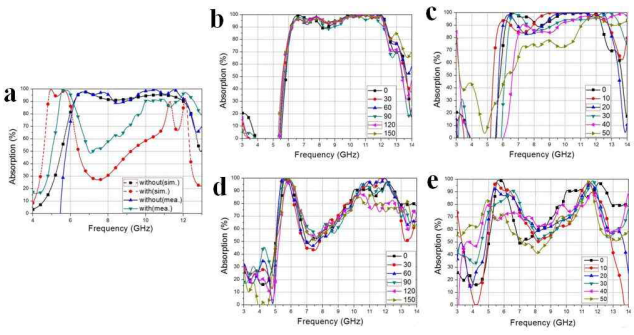

FIGURE 7. (a) Comparison of simulation and measurement results, measurement results of fabricated sample without EGaIn for different (b) polarizations and (c) incident angles, and with EGaIn for different (d) polarizations and (e) incident angles.

spectrum in the measurement result of the sample did not change, as shown in Figure 7b. For all polarization angles, the absorption of the metasurface sample without EGaIn was higher than 90% from 6.23 to 12.13 GHz. When the incident angle was increased, the absorption decreased, as shown in Figure 7c. The absorption of the sample metasurface was greater than 80% at 7 to 12 GHz when the incident angle was lower than 40°. Figure 7d and 7e shows the measurement results of the sample using EGaIn for different polarizations and incident angles, respectively. When the polarization was changed from zero to 180°, the measurement result of the sample did not change, as shown in Figure 7d. For all polarization angles, the absorption of the metasurface sample without EGaIn was higher than 90% at 5.44 to 6.12 GHz. When the incident angle was increased, the absorption decreased, as shown in Figure 7e. The absorption was greater than 80% at 5.35 to 6.12 GHz at an incident angle lower than 40°.

IV. CONCLUSION

In this paper, we proposed a fluidically switchable liquid metal metasurface for broadband and polarization-insensitive absorption. To realize a wide absorption spectrum, we used a chip resistor, and to realize the switchability, we used a microfluidic channel and liquid metal. The top metallic pattern consisted of a four-circular sector and isolated patches. When liquid metal was not injected into the microfluidic channel, only the four-circular sector operated and absorbed electromagnetic waves at 6 to 12 GHz. When liquid metal was injected into the microfluidic channel, the channel connected the four-circular sector and the isolated patches and the electromagnetic wave absorption spectrum shifted to 5 to 6 GHz. We fabricated a sample of 10 × 10 unitcells to measure the performance of the proposed metasurface. When liquid metal was injected, the absorption spectrum showed absorptivity of greater than 90% at 6.23 to 12.13 GHz. When liquid metal was not injected, the absorption spectrum showed absorptivity of greater than 90% at 5.44 to 6.12 GHz. The proposed metasurface exhibited an incident angle insensitivity regardless of whether the liquid metal was injected. When the polarization was changed, the measurement result of the proposed metasurface showed no difference.

Table 1 compares the proposed frequency switchable metasurface with previous switchable metasurfaces used in other papers. For this comparison, the fractional bandwidth (FBW) is defined as

$$\mathrm{FBW} = \frac{f_{highest} - f_{lowest}}{f_{center}} \times 100[\%], \tag{1}$$

where $f_{highest}$ and f_{lowest} are the highest and lowest frequencies when the absorption exceeds 90%, respectively. In addition, f_{center} is the center frequency between $f_{highest}$ and f_{lowest}. As a frequency switchable metasurface, two FBWs are given at low and high frequency bands. In addition, switching range (SR) is defined as

$$\mathrm{SR} = \frac{f_{c_high} - f_{c_low}}{f_{c_high}} \times 100[\%], \tag{2}$$

TABLE 1. Performance comparison of the proposed switchable metasurface absorber and other metasurface absorbers.

	FBW_L [%]	FBW_H [%]	SR [%]	Polarization Insensitivity	Angle Insensitivity	Switching Technology
Proposed metasurface	12.9	64.3	54	Insensitive	Insensitive	Liquid metal
[20]	26	63.5	51	Sensitive	Insensitive	Liquid metal
[32]	10.2	13.2	10.2	Insensitive	N/A	PIN diode
[33]	17.4	74.7	73	Insensitive	Insensitive	PIN diode
[34]	3.2	3.6	20	Insensitive	N/A	Liquid crystal
[35]	1.7	1.9	46	N/A	N/A	MEMS
[36]	0	0	5	N/A	N/A	VO2
[37]	0	0	8	N/A	N/A	BST
[38]	1.1	0	16.1	Insensitive	N/A	Graphene

where f_{c-high} and f_{clow} are center frequencies at high and low frequency bands, respectively.

As shown in Table 1, compared to other frequency tuning methods, the proposed metasurface exhibits good performance in frequency switching and has the advantage of being insensitive to incident angles. Moreover, the proposed metasurface is insensitive to polarization compared to a metasurface using a conventional liquid metal.

REFERENCES

[1] J. Valentine *et al.*, "Three-dimensional optical metamaterial with a negative refractive index," *Nature*, vol. 455, no. 7211, pp. 376–379, Sep. 2008.
[2] N. Fang and X. Zhang, "Imaging properties of a metamaterial superlens," in *Proc. IEEE Conf. Nanotechnol.*, Aug. 2002, pp. 225–228.
[3] J. Zhu and G. V. Eleftheriades, "A compact transmission-line metamaterial antenna with extended bandwidth," *IEEE Antennas Wireless Propag. Lett.*, vol. 8, pp. 295–298, 2009.
[4] A. Alu and N. Engheta, "All optical metamaterial circuit board at the nanoscale," *Phys. Rev. Lett.*, vol. 103, no. 14, pp. 2–5, Sep. 2009.
[5] C. M. Watts, X. Liu, and W. J. Padilla, "Metamaterial electromagnetic wave absorbers," *Adv. Mater.*, vol. 24, no. 23, pp. OP98–OP120, 2012.
[6] K. Bi, L. Zeng, H. Chen, C. Fang, Q. Wang, and M. Lei, "Magnetic coupling effect of Mie resonance-based metamaterial with inclusion of split ring resonators," *J. Alloys Compound*, vol. 646, pp. 680–684, Oct. 2015.
[7] Y. Guo, J. Li, X. Hou, X. Lv, H. Liang, and J. Zhou, "A simple topology metamaterial blackbody for visible light," *J. Alloys Compound*, vol. 699, pp. 998–1002, Mar. 2017.
[8] P. Rufangura and C. Sabah, "Design and characterization of a dual-band perfect metamaterial absorber for solar cell applications," *J. Alloys Compound*, vol. 671, pp. 43–50, Jun. 2016.
[9] Z. Yang, F. Luo, W. Zhou, D. Zhu, and Z. Huang, "Design of a broadband electromagnetic absorbers based on TiO_2/Al_2O_3 ceramic coatings with metamaterial surfaces," *J. Alloys Compound*, vol. 687, pp. 384–388, Dec. 2016.
[10] N. I. Landy, S. Sajuyigbe, J. J. Mock, D. R. Smith, and W. J. Padilla, "Perfect metamaterial absorber," *Phys. Rev. Lett.*, vol. 100, no. 20, pp. 207402-1–207402-4, 2008.
[11] O. M. Bucci and G. Franceschetti, "Scattering from wedge-tapered absorbers," *IEEE Trans. Antennas Propag.*, vol. 19, no. 1, pp. 96–104, Jan. 1971.
[12] E. F. Knott and C. D. Lunden, "The two-sheet capacitive Jaumann absorber," *IEEE Trans. Antennas Propag.*, vol. 43, no. 11, pp. 1339–1343, Nov. 1995.

[13] J. W. Park *et al.*, "Multi-band metamaterial absorber based on the arrangement of donut-type resonators," *Opt. Express*, vol. 21, no. 8, pp. 9691–9702, 2013.
[14] B. Wang, B. Y. Gong, M. Wang, B. Weng, and X. Zhao, "Dendritic wideband metamaterial absorber based on resistance film," *Appl. Phys. A, Mater. Sci. Process.*, vol. 118, no. 4, pp. 1559–1563, 2014.
[15] B. Zhu, C. Huang, Y. Feng, J. Zhao, and T. Jiang, "Dual band switchable metamaterial electromagnetic absorber," *Prog. Electromagn. Res. B*, vol. 24, pp. 121–129, Aug. 2010.
[16] C. Yong-Zhi, G. Rong-Zhou, N. Yan, and W. Xian, "A wideband metamaterial absorber based on a magnetic resonator loaded with lumped resistors," *Chin. Phys. B*, vol. 21, no. 12, p. 127801, 2012.
[17] J. Zhao, Q. Cheng, J. Chen, M. Q. Qi, W. X. Jiang, and T. J. Cui, "A tunable metamaterial absorber using varactor diodes," *New J. Phys.*, vol. 15, p. 043049, Apr. 2013.
[18] D. Shrekenhamer, W.-C. Chen, and W. J. Padilla, "Liquid crystal tunable metamaterial absorber," *Phys. Rev. Lett.*, vol. 110, no. 17, pp. 177403-1–177403-5, 2013.
[19] F. Hu *et al.*, "Design of a tunable terahertz narrowband metamaterial absorber based on an electrostatically actuated MEMS cantilever and split ring resonator array," *J. Opt.*, vol. 15, no. 5, p. 055101, 2013.
[20] J. Liang, X. Song, J. Li, K. Lan, and P. Li, "A visible-near infrared wavelength-tunable metamaterial absorber based on the structure of Au triangle arrays embedded in VO_2 thin film," *J. Alloys Compound*, vol. 708, pp. 999–1007, Jun. 2017.
[21] Y. Bian, C. Wu, H. Li, and J. Zhai, "A tunable metamaterial dependent on electric field at terahertz with barium strontium titanate thin film," *Appl. Phys. Lett.*, vol. 104, no. 4, p. 042906, 2014.
[22] A. Andryieuski and A. V. Lavrinenko, "Graphene metamaterials based tunable terahertz absorber: Effective surface conductivity approach," *Opt. Express*, vol. 21, no. 7, pp. 9144–9155, 2013.
[23] K. Ling, H. K. Kim, M. Yoo, and S. Lim, "Frequency-switchable metamaterial absorber injecting eutectic gallium-indium (EGaIn) liquid metal alloy," *Sensors*, vol. 15, no. 11, pp. 28154–28165, 2015.
[24] H. K. Kim, D. Lee, and S. Lim, "Wideband-switchable metamaterial absorber using injected liquid metal," *Sci. Rep.*, vol. 6, no. 1, p. 31823, 2016.
[25] D. Lee, J. G. Hwang, D. Lim, T. Hara, and S. Lim, "Incident angle- and polarization-insensitive metamaterial absorber using circular sectors," *Sci. Rep.*, vol. 6, Jun. 2016, Art. no. 27155.
[26] T. T. Nguyen and S. Lim, "Angle- and polarization-insensitive broadband metamaterial absorber using resistive fan-shaped resonators," *Appl. Phys. Lett.*, vol. 112, no. 2, p. 021605, 2018.
[27] S. Cheng, H. Yousef, and H. Kratz, "79 GHz slot antennas based on substrate integrated waveguides (SIW) in a flexible printed circuit board," *IEEE Trans. Antennas Propag.*, vol. 57, no. 1, pp. 64–71, Jan. 2009.
[28] K. Ling, K. Kim, and S. Lim, "Flexible liquid metal-filled metamaterial absorber on polydimethylsiloxane (PDMS)," *Opt. Express*, vol. 23, no. 16, pp. 21375–21383, 2015.
[29] N. J. Farcich, J. Salonen, and P. M. Asbeck, "Single-length method used to determine the dielectric constant of polydimethylsiloxane," *IEEE Trans. Microw. Theory Techn.*, vol. 56, no. 12, pp. 2963–2971, Dec. 2008.
[30] M. D. Dickey, R. C. Chiechi, R. J. Larsen, E. A. Weiss, D. A. Weitz, and G. M. Whitesides, "Eutectic gallium-indium (EGaIn): A liquid metal alloy for the formation of stable structures in microchannels at room temperature," *Adv. Funct. Mater.*, vol. 18, no. 7, pp. 1097–1104, Apr. 2008.
[31] G. Maier, "Low dielectric constant polymers for microelectronics," *Prog. Polym. Sci.*, vol. 26, no. 1, pp. 3–65, Feb. 2001.
[32] S. An *et al.*, "Design of a polarization-insensitive wideband tunable metamaterial absorber based on split semi-circle ring resonators," *J. Appl. Phys.*, vol. 122, no. 2, pp. 025113-1–025113-6, 2017.
[33] D. Lee, H. Jeong, and S. Lim, "Electronically switchable broadband metamaterial absorber," *Sci. Rep.*, vol. 7, no. 1, 2017, Art. no. 4891.
[34] G. Isić, B. Vasić, D. C. Zografopoulos, R. Beccherelli, and R. Gajić, "Electrically tunable critically coupled terahertz metamaterial absorber based on nematic liquid crystals," *Phys. Rev. Appl.*, vol. 3, no. 6, pp. 064007-1–064007-8, 2015.
[35] Q. Ye, H. Lin, X. Chen, and H. Yang, "A tunable metamaterial absorber made by micro-gaps structures," in *Proc. Cross Strait Quad-Regional Radio Sci. Wireless Technol. Conf.*, 2011, pp. 234–237.
[36] M. J. Dicken *et al.*, "Frequency tunable near-infrared metamaterials based on VO_2 phase transition," *Opt. Express*, vol. 17, no. 20, pp. 18330–18339, 2009.
[37] T. H. Hand and S. A. Cummer, "Frequency tunable electromagnetic metamaterial using ferroelectric loaded split rings," *J. Appl. Phys.*, vol. 103, no. 6, p. 066105, 2008.
[38] Y. Zhang, Y. Feng, B. Zhu, J. Zhao, and T. Jiang, "Graphene based tunable metamaterial absorber and polarization modulation in terahertz frequency," *Opt. Express*, vol. 22, no. 19, pp. 22743–22752, 2014.

DAECHEON LIM received the B.S. degree in electrical and electronics engineering from Chung-Ang University, Seoul, South Korea, in 2017, where he is currently pursuing the M.S. degree in electrical and electronics engineering.

His research interests are focused on metamaterial applications and microwave absorbers.

SUNGJOON LIM received the B.Sc. degree in electronic engineering from Yonsei University, Seoul, South Korea, in 2002, and the M.S. and Ph.D. degrees in electrical engineering from the University of California at Los Angeles, Los Angeles, CA, USA, in 2004 and 2006, respectively. After a post-doctoral position at the Integrated Nano system Research Facility, University of California at Irvine, he joined the School of Electrical and Electronics Engineering, Chung-Ang University, Seoul, in 2007, where he is currently a Professor. From 2013 to 2014, he was a Visiting Scholar with the Georgia Institute of Technology, Atlanta, GA, USA. He has authored and co-authored over 200 international conference, letter, and journal papers. His research interests include engineered electromagnetic structures (metamaterials, electromagnetic bandgap materials, and frequency selective surfaces), electromagnetic-based sensors, microfluidic RF electronics, inkjet-printed RF electronics, and RF MEMS applications. He received the Institution of Engineering and Technology Premium Award in 2009 and the ETRI Journal Best Paper Award in 2014. He achieved the CAU Distinguished Scholar Award for 2014–2018.